



UNIVERSITY OF LEEDS

This is a repository copy of *Kinetic studies of atmospherically relevant silicon chemistry Part I: Silicon atom reactions*.

White Rose Research Online URL for this paper:
<http://eprints.whiterose.ac.uk/87156/>

Version: Accepted Version

Article:

Martin, JCG orcid.org/0000-0001-7972-085X, Blitz, MA orcid.org/0000-0001-6710-4021 and Plane, JMC orcid.org/0000-0003-3648-6893 (2009) Kinetic studies of atmospherically relevant silicon chemistry Part I: Silicon atom reactions. *Physical Chemistry Chemical Physics*, 11 (4). pp. 671-678. ISSN 1463-9076

<https://doi.org/10.1039/b812946k>

© 2008, Royal Society of Chemistry. This is an author produced version of a paper published in *Physical Chemistry Chemical Physics*. Uploaded in accordance with the publisher's self-archiving policy.

Reuse

Unless indicated otherwise, fulltext items are protected by copyright with all rights reserved. The copyright exception in section 29 of the Copyright, Designs and Patents Act 1988 allows the making of a single copy solely for the purpose of non-commercial research or private study within the limits of fair dealing. The publisher or other rights-holder may allow further reproduction and re-use of this version - refer to the White Rose Research Online record for this item. Where records identify the publisher as the copyright holder, users can verify any specific terms of use on the publisher's website.

Takedown

If you consider content in White Rose Research Online to be in breach of UK law, please notify us by emailing eprints@whiterose.ac.uk including the URL of the record and the reason for the withdrawal request.



eprints@whiterose.ac.uk
<https://eprints.whiterose.ac.uk/>

Kinetic studies of atmospherically relevant silicon chemistry.

Part I: Silicon atom reactions

*Juan C. Gómez Martín, Mark A. Blitz and John M. C. Plane**

School of Chemistry, University of Leeds, LS2 9JT, UK,

*Correspondence to: J. M. C. Plane (j.m.c.plane@leeds.ac.uk)

Abstract

Atomic silicon is generated by meteoric ablation in the earth's upper atmosphere (70 – 110 km). The reactions of Si(³P_{*j*}) atoms with several atmospherically relevant species were studied by the pulsed laser photolysis of a Si atom precursor (typically PheSiH₃), followed by time-resolved laser induced fluorescence at 251.43 nm (Si(3*p*² ³P₀ → 4*s* ³P₁)). This yielded:

$k(\text{Si} + \text{O}_2, 190 - 500 \text{ K}) = 9.49 \times 10^{-11} + 1.80 \times 10^{-10} \times \exp(-T/115 \text{ K}) \text{ cm}^3 \text{ molecule}^{-1} \text{ s}^{-1}$ (uncertainty $\leq \pm 15\%$), in good accord with recent high-level theoretical calculations but in marked disagreement with previous experimental work; $k(\text{Si} + \text{O}_3, 190 - 293 \text{ K}) = (4.0 \pm 0.5) \times 10^{-10} \text{ cm}^3 \text{ molecule}^{-1} \text{ s}^{-1}$; $k(\text{Si} + \text{CO}_2, 293 \text{ K}) \leq 1.2 \times 10^{-14} \text{ cm}^3 \text{ molecule}^{-1} \text{ s}^{-1}$; and $k(\text{Si} + \text{H}_2\text{O}, 293 \text{ K}) \leq 2.6 \times 10^{-13} \text{ cm}^3 \text{ molecule}^{-1} \text{ s}^{-1}$. These results are explained using a combination of quantum chemistry calculations and long-range capture theory. The quenching rate coefficients $k(\text{Si}(^1\text{D}_2) + \text{N}_2, 293 \text{ K}) = (4.0 \pm 0.7) \times 10^{-11} \text{ cm}^3 \text{ molecule}^{-1} \text{ s}^{-1}$ and $k(\text{Si}(^1\text{D}_2) + \text{H}_2\text{O}, 293 \text{ K}) = (2.3 \pm 0.3) \times 10^{-10} \text{ cm}^3 \text{ molecule}^{-1} \text{ s}^{-1}$ were also determined.

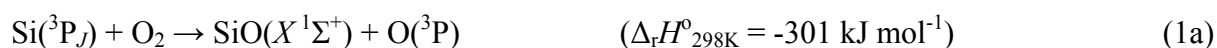
Key words: silicon atom, mesospheric chemistry, meteoric smoke.

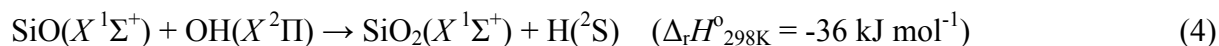
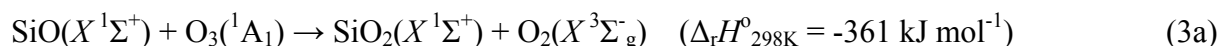
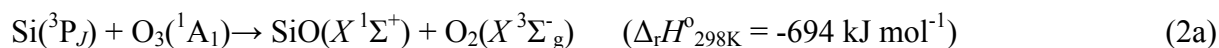
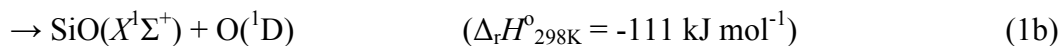
Introduction

The average input of interplanetary dust into the Earth's atmosphere is currently estimated to be about 40 tonnes d^{-1} .^{1,2} Most of these micron-sized dust particles ablate completely at altitudes between 75 km and 110 km, a region known as the mesosphere-lower thermosphere (MLT). The elemental abundance of silicon in meteorites is ~20%,³ so there should be a substantial input of silicon into the MLT. Ablation models predict that silicon will evaporate from molten meteoroids as a mixture of Si, SiO and SiO₂, a fraction of which will then be ionised by hyperthermal collisions with atmospheric molecules.⁴ Indeed, Si⁺ has been observed by rocket-borne mass spectrometers in the MLT,⁵ although most silicon species below 95 km are expected to be neutral as a result of rapid reactions of Si⁺ with O₃ and O₂, followed by dissociative recombination with electrons.^{6,7}

Silicon, iron and magnesium ablated from meteoroids are quickly oxidized and most likely re-condense to form nanometre-sized particles known as meteoric smoke particles (MSPs).⁸ MSPs probably act as ice nuclei for the formation of noctilucent clouds in the summer polar mesosphere,⁹ and may also be an important source of condensation nuclei for sulphate particles in the lower stratosphere and hence influence polar stratospheric cloud formation.¹⁰ In addition, MSP are alkaline, so they could explain the anomalous removal of H₂SO₄ in the upper stratosphere.¹¹ In order to determine the detailed composition of MSP (which will influence their ability to condense water-ice and react with acidic gases) and to quantify their rate of formation, knowledge of the speciation of silicon oxides as a function of altitude is needed.

The gas-phase oxidation of silicon is likely to proceed through the following reactions (the reaction enthalpies are taken from ref. 12,13):





The silicon atom in SiO_2 has a tendency to increase its coordination number to 4 because of its $3d$ orbitals, and so SiO_2 is unstable with respect to forming bonds with adjacent SiO_2 molecules, giving rise to large polymers and finally to particles.^{14,15} This tendency to polymerise makes the hypothesis of silica being a precursor of MSPs very appealing. The formation of silica particles is also well known in the context of semiconductor technology.¹⁶ A recent study of MSP analogues also reports the formation of silica particles from the broadband photolysis of tetraethyl *ortho*-silicate (TEOS) in the presence of O_2 and O_3 .⁸

A study of the reactivity of atomic silicon towards simple molecules (O_2 , CO_2 , N_2O) was carried out by Husain and Norris in the broader context of investigating the relationship between electronic structure and atomic reactivity, particularly the role of spin-orbit coupling in atomic reactions.^{17,18} However, gas-phase kinetic studies of silicon atom reactions are relatively scarce,¹⁹ and surprisingly no data has been reported for reaction 2. reaction 1 has been studied a number of times, but there is disagreement in the room-temperature rate coefficient by more than one order of magnitude,^{17,18,20,21} and there has been only one study of the temperature dependence.²¹ Two recent theoretical determinations of k_1 tend to support the most recent measurements.^{22,23} There do not appear to be any experimental kinetic studies on SiO reactions.

The present paper is the first part of a study on neutral silicon chemistry relevant to planetary atmospheres. Here we describe an experimental and theoretical study of reactions 1 and 2, together with the following reactions:



The second part of this study²⁴ will focus on SiO chemistry (reactions 3 and 4).

Experimental Setup

Apparatus

The experimental system used in this work is a modified version of an apparatus used in previous studies on metal chemistry.^{25,26} Si atoms were generated in a slow flow reactor by the pulsed multiphoton dissociation at 193 nm (ArF excimer laser, Lambda Physik, COMPEX 102) of organo-silicon vapour in the presence of an excess of O₂, O₃, H₂O or CO₂. Si(³P_J) was observed by laser induced fluorescence (LIF) spectroscopy using a frequency-doubled Nd-YAG pumped dye laser (Sirah, CBR-G-30). The dye laser beam was orthogonal to the excimer beam (*cf.* the collinear alignment in figure 1 of Plane and Rollason²⁵), and intersected the excimer beam approximately 10 cm beyond the focal point of a lens (focal length = 50 cm) used to focus the excimer beam. Time scans of the concentration of silicon atoms were obtained by varying the time delay between the dye laser and the excimer pulse. For each time delay, the LIF signal corresponds to the average of 5 laser shots.

LIF was collected through an interference filter ($\lambda_{\text{max}} = 250$ nm, FWHM = 10 nm) using a photomultiplier tube (Electron Tubes, model 9816QB) placed orthogonal to both the photolysis and probe beams. Si(³P_J) was detected resonantly in the $J = 0, 1$ and 2 spin-orbit

states by exciting the transitions $3p^2\ ^3P_0 \rightarrow 4s\ ^3P_1$ (251.43 nm), $3p^2\ ^3P_1 \rightarrow 4s\ ^3P_2$ (250.69 nm) and $3p^2\ ^3P_2 \rightarrow 4s\ ^3P_2$ (251.61 nm). The first electronic excited state Si(1D_2) was also detected resonantly using the $3p^2\ ^1D_2 \rightarrow 4s\ ^1P_1$ transition at 288.16 nm.

The concentrations of O₃ and PheSiH₃ were monitored by UV absorption spectroscopy between 250 nm and 300 nm using a 1 m long absorption cell situated downstream from the reactor. The broad band radiation of a deuterium lamp (Hamamatsu) was passed through the absorption cell and focussed into the 200 μm wide entrance slit of a 0.5 m grating spectrometer (Spex, model 1870B) equipped with a 1200 groove mm⁻¹ grating (resolution 0.12 nm FWHM). Absorption spectra were recorded with a photodiode array (EG&G, PARC 1412) and converted to optical density, before fitting reference absorption cross sections for O₃ and PheSiH₃ to derive their concentrations.^{27,28}

The concentrations of O₂, CO₂ and organo-silicon vapour were calculated from the mass flow rates and absolute pressure in the reactor. Diluted mixtures of these species were prepared in a glass vacuum line by making them up to a known ratio in about 800 Torr of bath gas (N₂ or He) in 10 dm³ glass bulbs. H₂O vapour was generated by bubbling the buffer gas, helium, through de-ionised H₂O to entrain its vapour pressure in the main gas flow. The water concentration was determined from its saturated vapour pressure at 293 K (17.54 Torr) and the backing He pressure (typically 800 Torr). Kinetic experiments were performed by releasing controlled flows of the stored reactants and the bath gas through calibrated flow controllers (MKS) into a mixing manifold, and then delivering the mixture to the reactor in three different ports to allow homogeneous mixing. The precursor mixture was delivered through a flow controller directly to the reactor to avoid long contact times with the reactants. The total flow through the reactor was typically 500 standard cm³ s⁻¹ (sccm), at pressures between 4 and 20 Torr. At 4 Torr, where most experiments were performed, the typical

residence time of the gas mixture in the reactor was less than 200 ms. At a laser repetition rate of 5 Hz, this ensured a fresh gas mixture at each excimer pulse.

The reactor was enclosed in an electrically heated furnace, which could be also be filled with solid CO₂ to cool it, providing a temperature range from 190 K to 500 K. A permanently inserted chromel-alumel thermocouple was used to monitor the temperature inside the central chamber of the reactor, about 1.5 cm below the intersection of the laser beams.

Materials

He (99.9999 %, BOC Gases), N₂ (99.9999 %, BOC Gases) and O₂ (99.999 %, BOC Gases) were used without further purification. CO₂ was evaporated from solid CO₂ (99.995 %, BOC Gases), which had been previously pumped on for several minutes. O₃ was made by flowing O₂ through a commercial ozonizer (Fischer, OZ500) to produce a 5 % O₃ in O₂ mixture. The mixture was collected on silica gel held at 177 K by an ethanol slush bath, and O₂ was then pumped off at the same temperature. Deionised H₂O was obtained from a commercial de-ioniser (Purite). PheSiH₃ and SiBr₄ (Sigma Aldrich) were initially degassed by freeze-pump-thawing to remove volatile contaminants, although it was shown that this purification step did not affect the measured rate coefficients.

Results

Several silicon-containing organic compounds were tested as suitable photolytic precursors of atomic Si at 193 nm. Si atoms were not observed after photolysis of tetraethyl *ortho*-silicate (TEOS, Si(OC₂H₅)₄), and a poor yield resulted from photolysis of tetramethylsilane (TMS, Si(CH₃)₄). Phenylsilane (PheSiH₃) has a large cross section at 193 nm²⁸ and generated a

substantial Si signal, so it was used as the precursor in most experiments. Alternatively, silicon tetrabromide (SiBr_4)²⁹ was used in some experiments while studying reactions 1 and 2 to confirm that the precursor did not influence the measured rate coefficients.

Thermalisation of the $\text{Si}(^3\text{P}_J)$ spin-orbit population and quenching of $\text{Si}(^1\text{D}_2)$

The $J = 1$ and $J = 2$ spin-orbit states of $\text{Si}(^3\text{P}_J)$ lie 0.92 and 2.67 kJ mol^{-1} above the $J = 0$ level, respectively. As Le Picard *et al.*²¹ have pointed out, laser focusing results in a large amount of energy being concentrated into the small volume where the Si is formed, and therefore an initially non-Boltzmann spin-orbit population of the $\text{Si}(^3\text{P}_J)$ ground state would be expected, as well as the production of excited electronic states of Si. An experiment was therefore performed to check that the ground state spin-orbit level populations were thermalised. Photolysis of PheSiH_3 in 4 Torr of N_2 showed that over the decay time of the Si atom (~ 1 ms), the ratios of the LIF signals recorded for the $J = 0, 1, 2$ levels showed no deviation from the Boltzmann distribution, demonstrating that under these experimental conditions ground-state Si was fully thermalised. This was further confirmed by measuring k_1 by monitoring each of the spin-orbit states, which gave essentially the same result (see below).

We also confirmed that the first electronic excited state of silicon, $\text{Si}(^1\text{D}_2)$, lying 75 kJ mol^{-1} above the ground state, was quenched rapidly on the timescale of the kinetic measurements. A diluted mixture of N_2 in He was prepared and admitted into the reactor together with a larger flow of He. The decays of $\text{Si}(^1\text{D}_2)$ in the presence of excess N_2 were single exponentials, yielding a quenching rate coefficient $k(\text{Si}(^1\text{D}_2) + \text{N}_2, 293 \text{ K}) = (4.0 \pm 0.7) \times 10^{-11} \text{ cm}^3 \text{ molecule}^{-1} \text{ s}^{-1}$. The quoted uncertainty is the statistical error derived from weighted linear least squares fits to the $\ln[\text{LIF signal}]$ vs. time curves and the plot of the resulting pseudo first-order decay, k' , against $[\text{N}_2]$, where the uncertainty in the abscissa is also propagated in the

weighting matrix. Typically, quenching of Si(1D_2) by 4 Torr of N₂ takes place within 0.2 μ s after the photolysis pulse, whereas the time scale of the reactions under study is tens to hundreds of μ s.

Removal of Si(1D_2) by water was also observed, with a removal rate coefficient $k(\text{Si}(^1D_2) + \text{H}_2\text{O}, 293 \text{ K}) = (2.3 \pm 0.3) \times 10^{-10} \text{ cm}^3 \text{ molecule}^{-1} \text{ s}^{-1}$. SiO($X^1\Sigma^+$) + H₂($X^1\Sigma_g^+$) are accessible products of this reaction, but formation of SiO on the time scale of the Si(1D_2) decay was not observed (LIF detection of SiO is described in the second part of this study²⁴).

The reaction of Si(3P_J) with O₂

The rate coefficient of reaction 1, k_1 , was measured over the range of conditions summarized in Table 1. The decays of Si in the presence of O₂ were always single exponentials, so a linear fit of the logarithm of the LIF signal as a function of time (figure 1) provided directly the first-order decay rate at a given [O₂], k' . A plot of k' versus [O₂] gave k_1 , as shown in figure 2. The averaged values of k_1 at the four temperatures considered are: $k_1(190 \text{ K}) = (1.31 \pm 0.08) \times 10^{-10} \text{ cm}^3 \text{ molecule}^{-1} \text{ s}^{-1}$, $k_1(293 \text{ K}) = (1.03 \pm 0.10) \times 10^{-10} \text{ cm}^3 \text{ molecule}^{-1} \text{ s}^{-1}$, $k_1(400 \text{ K}) = (1.02 \pm 0.08) \times 10^{-10} \text{ cm}^3 \text{ molecule}^{-1} \text{ s}^{-1}$ and $k_1(500 \text{ K}) = (0.99 \pm 0.10) \times 10^{-10} \text{ cm}^3 \text{ molecule}^{-1} \text{ s}^{-1}$. Statistical errors both in k' and [O₂] are propagated in the quoted uncertainty at the 95% level.

The reaction of Si(3P_J) with O₃

A stock mixture of O₃ from silica gel was made up in N₂ in a 12 dm³ glass bulb. However, the O₃ also contained some fraction of O₂, and because reaction 1 is fast this fraction had to be determined. The [O₃] that should have been in the reactor, if the O₃ in the glass bulb was pure, was calculated from the ratio of O₃ in N₂ in the stock mixture, the mass flow rates and

the pressure in the reactor. $[O_3]$ was also spectroscopically determined in the gas flow exiting the reactor. The difference between these two quantities then provides an estimate of $[O_2]$ in the reactor. Under first-order conditions, k_2 was calculated by fitting a straight line to a plot of k' , corrected for the contribution from reaction 1, against $[O_3]$:

$$k'_{O_3} \equiv k' - k_1[O_2] = C + k_2[O_3] \quad (I)$$

where C is a constant measured for every set of precursor and reactant gas mixtures. Figure 3 shows plots of the logarithm of the LIF signal as a function of time for different $[O_3]$, and figure 4 is a bimolecular plot of the corrected first-order decay rates k'_{O_3} as a function of $[O_3]$. For comparison, k' is also plotted with k'_{O_3} . O_2 was found to comprise between 30% and 60% of the total gas released from the cooled silica gel trap when the O_3/N_2 mixture was made up. Note that in the example shown in figure 4 (where the fraction of O_2 was $(33 \pm 2)\%$, if k_2 were derived directly from k' without correcting for the contribution from reaction 1, then it would be overestimated by 14%. Table 2 summarises the experimental conditions over which k_2 was measured. No significant variation of the rate coefficient could be discerned within error over the temperature range examined, and so the weighted average is given by $k_2(190 \text{ K} - 293 \text{ K}) = (4.0 \pm 0.5) \times 10^{-10} \text{ cm}^3 \text{ molecule}^{-1} \text{ s}^{-1}$.

The reaction of Si(³P_J) with CO₂ and H₂O

Reactions 5 and 6 were studied with maximum $[CO_2] = (5.6 \pm 0.3) \times 10^{16} \text{ molecule cm}^{-3}$ and maximum $[H_2O] = (2.6 \pm 0.5) \times 10^{15} \text{ molecules cm}^{-3}$ (the estimated uncertainty in the water concentration takes into account potential wall losses). However, in both cases there was not a significant increase in k' compared to the decay rate in the absence of reactant. Taking account of the uncertainties in k' , the following upper limits were obtained: $k(\text{Si} + \text{CO}_2, 293$

K, 4 Torr) $\leq 1.2 \times 10^{-14}$ cm³ molecule⁻¹ s⁻¹ and $k(\text{Si} + \text{H}_2\text{O}, 293 \text{ K}, 10 \text{ Torr}) \leq 2.6 \times 10^{-13}$ cm³ molecule⁻¹ s⁻¹.

Discussion

Si(³P_{*J*}) + O₂

The results obtained for k_1 are plotted in figure 5 as a function of temperature, together with the results of previous studies.^{18,20,21} The negative temperature dependence of k_1 has been previously explained on the barrierless potential energy surface (PES).^{22,23} The reaction is then governed by the long-range part of the potential and depends on the population of the spin-orbit fine structure levels of the reactants in the entrance channel. Assuming negligible mixing of states during collisions,^{30,31} the reactivity depends on the thermal population of the four lowest spin-orbit states of the reactants, which connect to two reactive states: one to the ground state ¹A' and three to the ³A' excited state.²³ The 4 lowest states in the entrance channel and their corresponding degeneracies (*g*) are: Si(³P_{*J=0*}) + O₂(*X* ³Σ_{*g*}⁻, Ω=0) (*g*=1), Si(³P_{*J=0*}) + O₂(*X* ³Σ_{*g*}⁻, Ω=1) (*g*=2) and Si(³P_{*J=1*}) + O₂(*X* ³Σ_{*g*}⁻, Ω=0) (*g*=3, one state out of three). An increase in temperature depopulates these low energy states which lead to reaction, thus causing a decrease of k_1 .

The capture rate coefficient, which provides an upper limit to k_1 , was estimated in the present study using the simple dispersion force model with a $-C_6 r^{-6}$ attractive potential (“hard spheres with attraction”³²):

$$k(T) = \pi d^2 \Gamma(2/3) \left(\frac{2C_6}{kT} \right)^{1/3} \left(\frac{8kT}{\pi\mu} \right)^{1/2} \quad (\text{II})$$

where d is the hard sphere diameter and μ is the reduced mass. The C_6 coefficient was estimated to be $6.0 \times 10^{-54} \text{ J m}^{-6} \text{ molecule}^{-1}$ using the London Formula with tabulated polarisabilities and ionisation potentials.³³ On the other hand, the statistical population factor, also called multiple surface coefficient,³⁴ which assumes adiabatic correlation of reactants and products, varies from 0.33 to 0.21 over the temperature range 190 to 500 K. The *total* capture rate coefficient is given by the following expression:^{23,31}

$$k(T) = k_{\text{capt}}(T) \times [1 + e^{-111/T} + 2 \times e^{-5.7/T}] \times [1 + 3 \times e^{-111/T} + 5 \times e^{-321/T}]^{-1} \times [1 + 2 \times e^{-5.7/T}]^{-1} \quad (\text{III})$$

where $k_{\text{capt}}(T)$ indicates the capture rate constant and the numbers appearing in the exponents are the spin-orbit splitting equivalent temperatures for silicon and molecular oxygen. Equation III is for the singlet state and incorporates the triplet by assuming it has equal reactivity. The rate coefficients calculated according to equations II and III agree well with the temperature dependence and absolute values of k_1 measured in the present study from 190 to 500 K, as shown in figure 5.

Figure 5 also illustrates that the total capture rate coefficient is in good agreement with the values determined using the more sophisticated Adiabatic Capture Centrifugal Sudden Approximation (ACCSA)²² and Quasi-classical Trajectory (QCT)²³ approaches. This emphasises that the reaction is controlled by the long-range part of the potential, where the PES is more isotropic, in contrast to short-range interactions (distance of Si to X, where X is at the centre-of-mass of the O₂, is less than 3 Å) where there is a strong dependence on the Jacobi angle (the angle between Si-X and the O-O axis). We performed a calculation of the long-range part of the singlet PES ($r(\text{Si-X}) > 4 \text{ Å}$) at the B3LYP/6-311+G(2d,p) level of theory, using the Gaussian 03 suite programs.³⁵ C_6 coefficients were fitted to this surface for the range of Jacobi angles (0 – 90°): the variation of less than 40% in C_6 confirmed that there is not a very strong dependence on the Jacobi angle (see electronic supporting information). The angle-averaged C_6 is $3.9 \times 10^{-54} \text{ J m}^{-6} \text{ molecule}^{-1}$, which agrees reasonably well with the

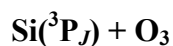
value calculated with the London formula (see above). If the total capture rate coefficient is fitted to the experimental points by making C_6 an adjustable parameter (green points in figure 5), the fitted C_6 value of $4.4 \times 10^{-54} \text{ J m}^{-6} \text{ molecule}^{-1}$ agrees extremely well with that derived from the quantum chemistry calculations. A temperature dependent expression for k_1 in the range 190 to 500 K has been derived by fitting an exponential function to the adjusted total capture rate coefficient:

$$k_1(190 - 500 \text{ K}) = 9.49 \times 10^{-11} + 1.80 \times 10^{-10} \times \exp(-T/115 \text{ K}) \text{ cm}^3 \text{ molecule}^{-1} \text{ s}^{-1} \quad (\text{IV})$$

Values obtained from this expression are shown in figure 5 (green solid line). The maximum uncertainty (green dashed lines) is 15%. This encompasses the quoted error bars for the experimental values of k_1 and the statistical errors associated to the fit to the London expression and the fit to the exponential function.

The negative temperature dependence of k_1 observed by Le Picard et al.²¹ is confirmed in the present study between 190 K and 293 K, and measurements have been extended up to 500 K. However, previous measurements of k_1 close to room temperature are widely scattered, ranging from about 1×10^{-11} to $2.7 \times 10^{-10} \text{ cm}^3 \text{ molecule}^{-1} \text{ s}^{-1}$ (figure 5). Although the results of the present study are in closest agreement with those of Le Picard et al., our results are systematically smaller by $\sim 40\%$, for which there is no obvious explanation.

The theoretical estimates of k_1 agree extremely well with the results of the present study (figure 5), which supports the idea that the reaction cross sections on the singlet and triplet PESs are of similar magnitude.²³ A recent experimental study of the dynamics of reaction 1 has confirmed for the first time the existence of channel 1a.³⁶ However, this was a crossed molecule beam study where the effective translation temperature is high and the observed $\text{O}(^3\text{P})$ signal was not quantified. Also, this study did not report detection of $\text{O}(^1\text{D})$, so even a relative reactivity of the triplet and singlet product channels cannot be assessed.



This reaction does not appear to have been studied previously. The rate coefficient is ~20% less than the upper limit of $5.4 \times 10^{-10} \text{ cm}^3 \text{ molecule}^{-1} \text{ s}^{-1}$ at 293 K calculated using the simple dispersion force model (figure 6). k_2 also has a small temperature dependence, consistent with calculations on the lowest (triplet) PES (at the B3LYP/6-311+G(2d,p) level of theory) which show a strongly attractive surface with no barriers over all angles of attack of Si on O_3 . Under C_s symmetry, when the Si attacks in the plane of the O_3 where the intermolecular forces are strongest, collisions between $\text{Si}(^3\text{P})$ and O_3 will occur on three PESs: two of $^3\text{A}''$ symmetry and one of $^3\text{A}'$ symmetry. As shown in figure 7, the lowest $^3\text{A}''$ surface correlates with the ground-state products $\text{SiO}(X^1\Sigma^+) + \text{O}_2(X^3\Sigma_g^-)$. The $^3\text{A}'$ surface and the second $^3\text{A}''$ surfaces correlate respectively with $\text{SiO}(C^1\Sigma^+) + \text{O}_2(X^3\Sigma_g^-)$ and $\text{SiO}(D^1\Delta) + \text{O}_2(X^3\Sigma_g^-)$, which are also exothermic reaction channels:^{37,38}



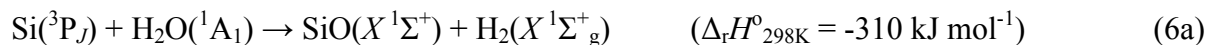
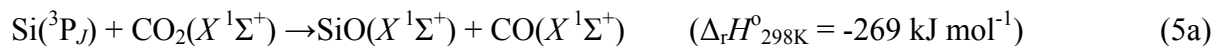
Therefore, all states in the entrance channel are directly correlated to exothermic product in C_s symmetry. However, k_2 is somewhat below the capture frequency (figure 6). This may be explained if only two of the three adiabatic triplet states generated by $\text{Si} + \text{O}_3$ are reactive, connecting with $2 \times 3 = 6$ out of 9 microstates. By analogy with equation III for reaction 1,²³ the total rate coefficient for reaction 2 would then be:

$$k(T) = k_{\text{capt}}(T) \times [1 + 3 \times e^{-111/T} + 2 \times e^{-321/T}] \times [1 + 3 \times e^{-111/T} + 5 \times e^{-321/T}]^{-1} \quad (\text{V})$$

Figure 6 shows that equation V yields sensible rate coefficients in the temperature interval studied experimentally.

Si(³P_J) + CO₂, H₂O

The bimolecular channels of reactions 5 and 6 are highly exothermic, but spin forbidden:



Calculations at the B3LYP/6-311+G(2d,p) level were therefore performed to explore the formation of possible collision adducts on the triplet PESs of these reactions. Accurate energies ($\pm 7 \text{ kJ mol}^{-1}$) were then calculated at the CBS-Q level of theory.^{39,40} As a benchmark, the heats of formation for SiO, SiO₂, SiH, SiH₂(¹A₁) and SiC calculated at this level of theory (Table 3) are in agreement with experimental determinations, taking into account that some experimental values have considerable uncertainty.^{12,37,41} In the case of reaction 5, formation of SiOCO and OSiCO is endothermic by 20 and 12 kJ mol⁻¹, respectively, which is consistent with the small upper limit to k_5 obtained in the present study. In contrast, Husain and Norris reported a large rate coefficient of $k_5 = (1.1 \pm 0.1) \times 10^{-11} \text{ cm}^3 \text{ molecule}^{-1} \text{ s}^{-1}$,¹⁸ which they explained by a non-adiabatic transition from the triplet reactant surface to the product singlet surface of reaction 5a. There is no obvious explanation for the discrepancy with the result of the present study of $k_5 \leq 1.2 \times 10^{-14} \text{ cm}^3 \text{ molecule}^{-1} \text{ s}^{-1}$. However, we note that Husain and co-workers^{42,43} did not observe the analogous spin-forbidden reaction between C(³P) and CO₂ to occur. Extrapolation to 293 K of the high temperature rate coefficients determined by Mick and Roth⁴⁴ (2100 K – 3160 K) is consistent with the room temperature upper limit reported in the present work.

Figure 8 is a potential energy diagram for reaction 6, which shows that formation of SiOH₂ and HSiOH is exothermic by -50 and -142 kJ mol⁻¹, respectively. However, insertion of Si into H₂O to form HSiOH involves a barrier of 34 kJ mol⁻¹. Although there is no barrier to formation of SiOH₂, this is a rather weakly-bound adduct and dissociation to SiO(*a*³Σ⁺) +

$\text{H}_2(X^1\Sigma_g^+)$ is endothermic ($\Delta_r H^0_{298\text{K}} = 93.7 \text{ kJ mol}^{-1}$ ^{37,45}). The quantum chemistry calculations therefore explain the small upper limit to k_6 measured in the present study at 10 Torr, although stabilization of SiOH_2 at higher pressures can be expected. There do not appear to have been any previous experimental studies of this reaction.

$\text{Si}(^1\text{D}_2) + \text{N}_2, \text{H}_2\text{O}$

Chemical reaction of $\text{Si}(^1\text{D}_2)$ with N_2 to yield $\text{SiN}(^2\Sigma) + \text{N}(^4\text{S})$ is spin forbidden and endothermic by 351 kJ mol^{-1} . However, a relatively fast removal of $\text{Si}(^1\text{D}_2)$ has been observed, indicating efficient physical quenching: $k(\text{Si}(^1\text{D}_2) + \text{N}_2, 293 \text{ K}) = (4.0 \pm 0.7) \times 10^{-11} \text{ cm}^3 \text{ molecule}^{-1} \text{ s}^{-1}$. This is in qualitative agreement with the observations of Le Picard et al.,²¹ who reported different behaviour of this species according to the nature of the buffer gas. From the approximate figures given by these authors a quenching rate coefficient larger than $10^{-11} \text{ cm}^3 \text{ molecule}^{-1} \text{ s}^{-1}$ can be estimated. Koi et al. reported formation of $\text{Si}(^3\text{P})$ in less than $1 \mu\text{s}$,⁴⁶ which they attributed to quenching of $\text{Si}(^1\text{D}_2)$ by 10 Torr of N_2 , implying a lower limit of $3 \times 10^{-12} \text{ cm}^3 \text{ molecule}^{-1} \text{ s}^{-1}$. On the other hand, Husain and Norris found an upper limit of $5 \times 10^{-12} \text{ cm}^3 \text{ molecule}^{-1} \text{ s}^{-1}$,⁴⁷ although they pointed out that reduction of signal with added N_2 limited the range of concentration that could be employed in their experiment.

$\text{Si}(^1\text{D}_2)$ is rapidly removed in the presence of H_2O ($k(\text{Si}(^1\text{D}_2) + \text{H}_2\text{O}, 293 \text{ K}) = (2.3 \pm 0.3) \times 10^{-10} \text{ cm}^3 \text{ molecule}^{-1} \text{ s}^{-1}$). The $\text{Si}(^1\text{D}_2) + \text{H}_2\text{O}$ reaction is analogous to the chemical reaction $\text{O}(^1\text{D}) + \text{H}_2\text{O}$, but the former is endothermic by $122.4 \text{ kJ mol}^{-1}$. The quantum calculations shown in figure 8 indicate that besides physical quenching there could be a significant contribution of chemical reaction to the removal of $\text{Si}(^1\text{D}_2)$. The minimum energy path on the singlet surface ends with the products $\text{SiO} + \text{H}_2$, although SiO was not observed (see above).

This suggests that reaction rather proceeds from the shallow SiOH_2 well straight to the products $\text{SiOH} + \text{H}$.

Atmospheric implications

In the atmosphere, meteoric ablation produces Si atoms, which will be oxidised to SiO very rapidly by O_2 : at the ablation peak around 90 km in the MLT region⁴ the lifetime of a Si atom will be ~ 0.3 ms. The relative abundance of O_3 to O_2 in the MLT ($\sim 3 \times 10^{-5}$) makes reaction 2 a minor process. As there are no exothermic processes to recycle SiO back to Si, the speciation of silicon depends only on reactions converting SiO into SiO_2 , and possibly SiOH or HSiOH. An investigation of these reactions is reported in the second part of this study.²⁴ A full mesospheric silicon model using these kinetic measurements and comparing with rocket-borne measurements⁵ will be published elsewhere.

Conclusions

The reactions of $\text{Si}(^3\text{P}_J)$ with O_2 and O_3 were found to be fast, and exhibited the characteristic features of barrierless capture-controlled processes: a negative temperature dependence for $\text{Si}(^3\text{P}_J) + \text{O}_2$, and insignificant temperature dependence for $\text{Si}(^3\text{P}_J) + \text{O}_3$. A comparison of the experimental rate coefficients to the adiabatic, multiple surface corrected capture rate coefficients provided some insights into the mechanisms of these reactions. The reactions of $\text{Si}(^3\text{P}_J)$ with CO_2 and H_2O were not observed, which is explained by the spin forbidden nature of the strongly exothermic channels and the existence of barriers or shallow wells on the spin conserving PESs.

Acknowledgements

This work was supported by the Natural Environment Research Council (grant NE/E005659/1).

TABLES

Table 1. Rate constants for reaction 1 and relevant experimental conditions (4 Torr N₂ in all cases)

T / K	J^a	$[O_2] / 10^{13} \text{ cm}^{-3}$	Precursor	$k_1 / 10^{-10} \text{ cm}^3 \text{ s}^{-1}$
190	0	2 – 260	PheSiH ₃	1.37±0.12
190	1	5 – 511	PheSiH ₃	1.30±0.09
190	2	5 – 511	PheSiH ₃	1.24±0.07
293	0	3 – 152	PheSiH ₃	0.96±0.09
293	0	8 - 460	SiBr ₄	1.19±0.07
400	0	13 - 127	PheSiH ₃	1.02±0.08
500	0	4 - 85	PheSiH ₃	0.99±0.10

^a Spin-orbit state

Table 2. Rate constants for reaction 2 and relevant experimental conditions ($J = 0$ and 4 Torr N₂ in all cases)

T / K	$[O_3] / 10^{13} \text{ cm}^{-3}$	$[O_2] / 10^{13} \text{ cm}^{-3}$	Precursor	$k / 10^{-10} \text{ cm}^3 \text{ s}^{-1}$
190	7-165	5-125	PheSiH ₃	4.2±0.4
293	4-75	1-85	PheSiH ₃	3.9±0.4
293	5-61	5-113	SiBr ₄	3.5±0.5

Table 3. Heats of formation (CBS-Q) of SiO, SiO₂, SiH, SiH₂, SiC, SiOCO, OSiCO, HSiOH and SiOH₂. For comparison, experimental values (where available) are shown in brackets.
12,13,37,48

Species ^a	$\Delta H_f^0(0\text{ K})$ (kJ mol ⁻¹) ^b	
SiO (¹ Σ^+)	-109.87	[-104.3±0.8 ¹³]
SiO ₂ (¹ Σ^+)	-295.09	[-305±33 ¹²] [-320.72 ⁴¹]
SiH (² Π_J)	366.20	[375±8 ¹²] [366.9 ⁴¹]
SiH ₂ (¹ A ₁)	264.30	[275±3 ¹³]
SiC ([*] 3 Π_J) ^c	731.4	[715±33 ¹²]
SiOCO (³ A)	63.30	
OSiCO (³ A'')	54.79	
SiOH (² A')	-7.80	
HSiO (² A')	19.32	
HSiOH- <i>cis</i> (¹ A')	-101.01	
HSiOH- <i>trans</i> (¹ A')	-101.09	
HSiOH (³ A)	67.65	
SiOH ₂ (¹ A')	240.40	
SiOH ₂ (³ A)	166.82	
H ₂ SiO (¹ A')	-104.35	

^a Optimized geometries and molecular constants at the B3LYP/6-311+G(2d,p) level of theory can be found in the supplementary electronic information. ^b Evaluated uncertainty = ± 7 kJ mol⁻¹.⁴⁰ The heats of formation at 0 K of the corresponding atomic species are: Si(³P), 446±8 kJ mol⁻¹; O(³P), 246.98±0.08 kJ mol⁻¹; H(²S), 216.164±0.004 kJ mol⁻¹; and C(³P), 711.7±0.4 kJ mol⁻¹.¹³ ^c The nature of the ground state is uncertain.⁴⁸

FIGURE CAPTIONS

Figure 1: Logarithm of silicon atoms fluorescence signal as a function of time at 293 K for different O₂ concentrations: no O₂ (■), 8.2 × 10¹³ molecules cm⁻³ (□), 4.9 × 10¹⁴ molecules cm⁻³ (▲), 1.2 × 10¹⁵ molecules cm⁻³ (Δ), 2.5 × 10¹⁵ molecules cm⁻³ (○) and 4.2 × 10¹⁵ molecules cm⁻³ (●).

Figure 2: Bimolecular plot (first order silicon decay rates k' as a function of O_2 concentration) for reaction 1 at 190 K (\square) and 400 K (\blacksquare).

Figure 3: Logarithm of silicon atoms fluorescence signal as a function of time at 190 K for different O_3 concentrations: no O_3 (\blacksquare), 7×10^{13} molecules cm^{-3} (\square), 2.2×10^{14} molecules cm^{-3} (\bullet), 2.9×10^{14} molecules cm^{-3} (\circ), 3.7×10^{14} molecules cm^{-3} (\blacktriangle), 5.3×10^{14} molecules cm^{-3} (\triangle), 7.0×10^{14} molecules cm^{-3} (\blacklozenge), 8.9×10^{14} molecules cm^{-3} (\diamond) and 1.5×10^{15} molecules cm^{-3} (\star).

Figure 4: First order silicon decay rates k' (\circ) and k'_{O_3} (\blacksquare) as a function of O_3 concentration (equation I) at 190 K. The gradients of the linear fits are $(4.93 \pm 0.12) \times 10^{-10}$ cm^3 molecules $^{-1}$ s $^{-1}$ and $(4.21 \pm 0.16) \times 10^{-10}$ cm^3 molecules $^{-1}$ s $^{-1}$ respectively. The uncertainty in $[O_3]$ (not shown) is 5% or smaller.

Figure 5: Comparison of the values obtained in the present study for k_1 (blue squares) to the experimental and theoretical values found in the literature (squares: experimental, triangles: theoretical). The thick red and black lines are fits to the experimental and theoretical data of the form $A \times T^{-B} \times e^{-C/T}$ in the range 15 K – 300 K.^{21,23} The dark green triangles correspond to the total capture rate coefficients obtained from the London Formula with C_6 derived from tabulated values. The light green triangles correspond to total capture rate coefficients for the optimal C_6 . The green line shows an empirical fit of these values (equation IV).

Figure 6: Comparison of the experimental values of $k(\text{Si} + O_3)$ (\blacksquare) to the capture upper limit rate coefficients (thick solid line). Total rate coefficients obtained using multiple surface factors for one and two reactive states are also shown (dashed and solid thin lines respectively).

Figure 7. Adiabatic correlations under C_s symmetry for co-planar attack of Si on O_3 .

Figure 8. Singlet and triplet PESs for Si + H₂O (thick and thin solid lines respectively) at CBS-Q level (± 7 kJ mol⁻¹). Calculated values reported in the literature are indicated by squares (referred to SiO+H₂).⁴⁹

References

- 1 D. W. Hughes, in *Cosmic Dust*, J. A. M. McDonnell, ed., 1978.
- 2 J. M. C. Plane, *Chem. Rev.*, 2003, **103**, 4963-4984.
- 3 C. Koeberl and E. H. Hagen, *Geochim. Cosmochim. Acta*, 1989, **53**, 937-944.
- 4 T. Vondrak, J. M. C. Plane, S. Broadley and D. Janches, *Atmos. Chem. Phys. Discuss.*, 2008, **8**, 14557-14606.
- 5 E. Kopp, H. Ramseyer and L. G. Bjoern, *Adv. Space Res.*, 1984, **4**, 157-161.
- 6 D. W. Fahey, F. C. Fehsenfeld, E. E. Ferguson and L. A. Viehland, *J. Chem. Phys.*, 1981, **75**, 669-674.
- 7 J. Fritzenwallner and E. Kopp, *Adv. Space Res.*, 1998, **21**, 891-894.
- 8 R. W. Saunders and J. M. C. Plane, *J. Atmos. Sol.-Terr. Phys.*, 2006, **68**, 2182-2202.
- 9 M. Rapp and G. E. Thomas, *J. Atmos. Sol.-Terr. Phys.*, 2006, **68**, 715-744.
- 10 D. J. Cziczo, D. S. Thomson and D. M. Murphy, *Science*, 2001, **291**, 1772-1775.
- 11 M. J. Mills, O. B. Toon, V. Vaida, P. E. Hintze, H. G. Kjaergaard, D. P. Schofield and T. W. Robinson, *J. Geophys. Res., [Atmos.]*, 2005, **110**, D08201/08201-D08201/08207.
- 12 M. W. Chase, Jr., *NIST-JANAF Thermochemical Tables*, 4th ed.; *J. Phys. Chem. Ref. Data*, Vol. 9, 1998.
- 13 L. A. Curtiss, K. Raghavachari, P. C. Redfern and J. A. Pople, *J. Chem. Phys.*, 1997, **106**, 1063-1079.
- 14 H. Schnoekel, *Z. Anorg. Allg. Chem.*, 1980, **460**, 37-50.

- 15 R. Janoschek, *J. Inorg. Organomet. Polym.*, 1993, **3**, 277-285.
- 16 D. M. Dobkin and M. K. Zuraw, *Principles of Chemical Vapor Deposition: What's Going on Inside the Reactor?*; Kluwer Academic Publishers, Dordrecht, 2003.
- 17 D. Husain and P. E. Norris, *J. Chem. Soc., Faraday Trans. II*, 1978, **74**, 93-105.
- 18 D. Husain and P. E. Norris, *J. Chem. Soc., Faraday Trans. II*, 1978, **74**, 106-114.
- 19 NIST, Chemical Kinetics Database, NIST Standard Reference Database, Release 1.4.11 2007, <http://kinetics.nist.gov/kinetics/index.jsp>
- 20 P. M. Swearingen, S. J. Davis and T. M. Niemczyk, *Chem. Phys. Lett.*, 1978, **55**, 274-279.
- 21 S. D. Le Picard, A. Canosa, G. Pineau des Forets, C. Rebrion-Rowe and B. R. Rowe, *Astron. Astrophys.*, 2001, **372**, 1064-1070.
- 22 S. D. Le Picard, A. Canosa, D. Reignier and T. Stoecklin, *Phys. Chem. Chem. Phys.*, 2002, **4**, 3659-3664.
- 23 F. Dayou and A. Spielfiedel, *J. Chem. Phys.*, 2003, **119**, 4237-4250.
- 24 J. C. Gómez Martín, M. A. Blitz and J. M. C. Plane, 2008, in preparation.
- 25 J. M. C. Plane and R. J. Rollason, *J. Phys. Chem. A*, 2001, **105**, 7047-7056.
- 26 J. M. C. Plane. in *Meteors in the Earth's Atmosphere. Meteoroids and Cosmic Dust and their Interactions with the Earth's Upper Atmosphere*, E. Murad and I. P. Williams, ed., Cambridge University Press, Cambridge, 2002.
- 27 J. P. Burrows, A. Richter, A. Dehn, B. Deters, S. Himmelmann, S. Voigt and J. Orphal, *J. Quant. Spectrosc. Radiat. Transfer*, 1999, **61**, 509-517.
- 28 A. Ioannidou-Philis, J. G. Philis and A. A. Christodoulides, *J. Mol. Spectrosc.*, 1987, **121**, 50-60.
- 29 J. B. Clark and B. R. Russell, *J. Electron Spectrosc. Relat. Phenom.*, 1977, **11**, 371-382.
- 30 D. G. Truhlar, *J. Chem. Phys.*, 1972, **56**, 3189-3190.

- 31 M. M. Graff and A. F. Wagner, *J. Chem. Phys.*, 1990, **92**, 2423-2439.
- 32 I. W. M. Smith, *Kinetics and Dynamics of Elementary Gas Reactions* Butterworths monographs in chemistry and chemical engineering; Butterworths, London, 1980.
- 33 D. R. Lide, Ed., *Handbook of Chemistry and Physics*, 73 ed.; CRC Press, Boca Raton, 1992.
- 34 J. T. Muckerman and M. D. Newton, *The Journal of Chemical Physics*, 1972, **56**, 3191-3192.
- 35 G. W. T. M. J. Frisch, H. B. Schlegel, G. E. Scuseria, M. A. Robb, J. R. Cheeseman, J. A. Montgomery, Jr., T. Vreven, K. N. Kudin, J. C. Burant, J. M. Millam, S. S. Iyengar, J. Tomasi, V. Barone, B. Mennucci, M. Cossi, G. Scalmani, N. Rega, G. A. Petersson, H. Nakatsuji, M. Hada, M. Ehara, K. Toyota, R. Fukuda, J. Hasegawa, M. Ishida, T. Nakajima, Y. Honda, O. Kitao, H. Nakai, M. Klene, X. Li, J. E. Knox, H. P. Hratchian, J. B. Cross, V. Bakken, C. Adamo, J. Jaramillo, R. Gomperts, R. E. Stratmann, O. Yazyev, A. J. Austin, R. Cammi, C. Pomelli, J. W. Ochterski, P. Y. Ayala, K. Morokuma, G. A. Voth, P. Salvador, J. J. Dannenberg, V. G. Zakrzewski, S. Dapprich, A. D. Daniels, M. C. Strain, O. Farkas, D. K. Malick, A. D. Rabuck, K. Raghavachari, J. B. Foresman, J. V. Ortiz, Q. Cui, A. G. Baboul, S. Clifford, J. Cioslowski, B. B. Stefanov, G. Liu, A. Liashenko, P. Piskorz, I. Komaromi, R. L. Martin, D. J. Fox, T. Keith, M. A. Al-Laham, C. Y. Peng, A. Nanayakkara, M. Challacombe, P. M. W. Gill, B. Johnson, W. Chen, M. W. Wong, C. Gonzalez, J. A. Pople, *Gaussian 03, Revision C.02*, Gaussian, Inc., Wallingford CT, 2004
- 36 R. Yamashiro, Y. Matsumoto and K. Honma, *J. Chem. Phys.*, 2008, **128**, 084308.
- 37 NIST, Computational Chemistry Comparison and Benchmark DataBase Release 14, NIST Standard Reference Database 101, 2006, <http://srdata.nist.gov/cccbdb>
- 38 R. W. Field, A. Lagerqvist and I. Renhorn, *Phys. Scr.*, 1976, **14**, 298-314.

- 39 J. W. Ochterski, G. A. Petersson and J. J. A. Montgomery, *J. Chem. Phys.*, 1996, **104**, 2598-2619.
- 40 L. A. Curtiss, K. Raghavachari, P. C. Redfern and B. B. Stefanov, *J. Chem. Phys.*, 1998, **108**, 692-697.
- 41 L. V. Gurvich, I. V. Veyts and C. B. Alcock, *Thermodynamic Properties of Individual Substances*, 4th ed.; Hemisphere Pub. Co., New York, 1989.
- 42 D. Husain and L. J. Kirsch, *Chem. Phys. Lett.*, 1971, **8**, 543-546.
- 43 D. Husain and A. N. Young, *J. Chem. Soc., Faraday Trans. II*, 1975, **71**, 525-531.
- 44 H. J. Mick and P. Roth, *J. Phys. Chem.*, 1994, **98**, 7844-7847.
- 45 G. Hager, R. Harris and S. G. Hadley, *J. Chem. Phys.*, 1975, **63**, 2810-2820.
- 46 M. Koi, K. Tonokura, A. Tezaki and M. Koshi, *J. Phys. Chem. A*, 2003, **107**, 4838-4842.
- 47 D. Husain and P. E. Norris, *J. Chem. Soc., Faraday Trans. II*, 1978, **74**, 1483-1503.
- 48 K. P. Huber, G. Herzberg, J. W. Gallagher and I. R.D. Johnson. in *NIST Chemistry WebBook, NIST Standard Reference Database Number 69*, E. P. J. Linstrom and W. G. Mallard, ed., National Institute of Standards and Technology, Gaithersburg MD, <http://webbook.nist.gov>, 2005.
- 49 M. R. Zachariah and W. Tsang, *J. Phys. Chem.*, 1995, **99**, 5308-5318.